Supporting Information

Electrostatic interactions-controlled dispersion of carbon nanotubes in ternary composite for high-performance supercapacitors

Jing Gao,[*a] Zhengyang Xing,[a] Junxi Zhou,[a] Haolan Xu,[a] Zhimin Wang,[a] Guohua Li,[a] and Lili Yu[*b]

[a] College of Chemical Engineering, Zhejiang University of Technology, Hangzhou 310014, P. R. China

[b] School of Material Science and Engineering, Shanghai University, Shanghai 200444, P. R. China

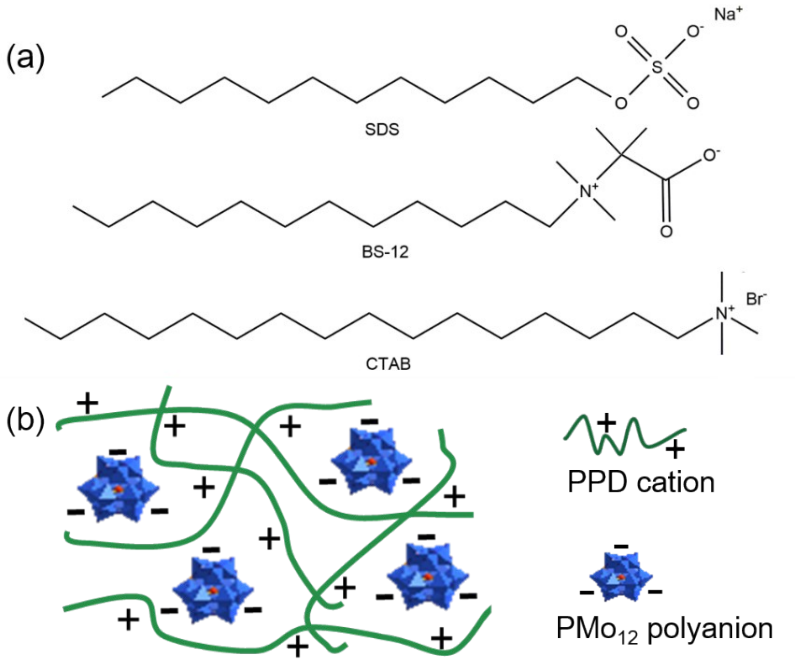

Figure S1. (a) Chemical structure of different ionic surfactants and (b) scheme image of PPD-PMo_{12} network.

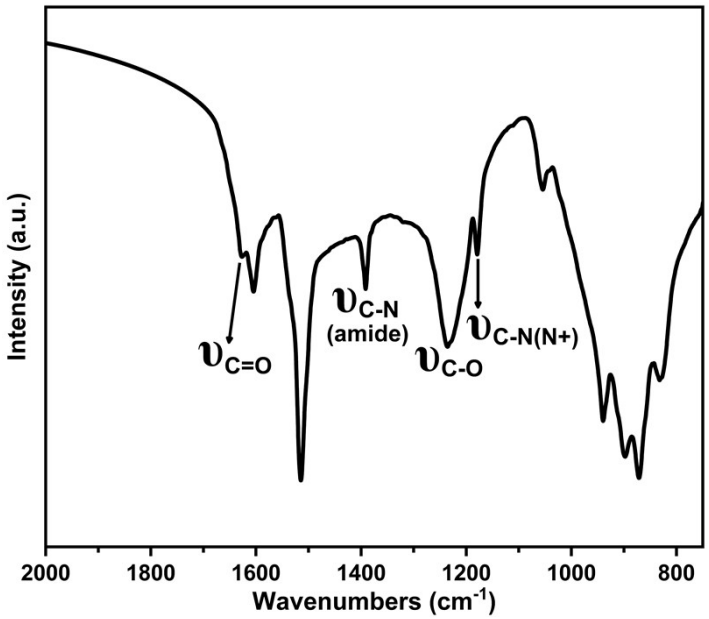

Figure S2 FTIR spectrum of DMoC.

FTIR spectrum of PPD-PMo_{12}@CNT (denoted as DMoC) shows characteristic peak of amide C=O (1624 cm^{-1}) and amide C–N (1391 cm^{-1}), indicating **CNT and PPD-PMo_{12} were covalently connected**. The formation mechanism of DMoC is as follows: the PMo_{12} with strong oxidative ability first initializes the polymerization of p-phenylenediamine (p-PD) to PPD and itself transforms to reduced-PMo_{12}. On addition of carboxylated CNT, the reduced-PMo_{12} turns back to PMo_{12} by reducing the CNT. Meanwhile, the PPD polymer with abundant amine groups forms amide bonds with CNT containing carboxyl groups, leading to formation of the DMoC composite.

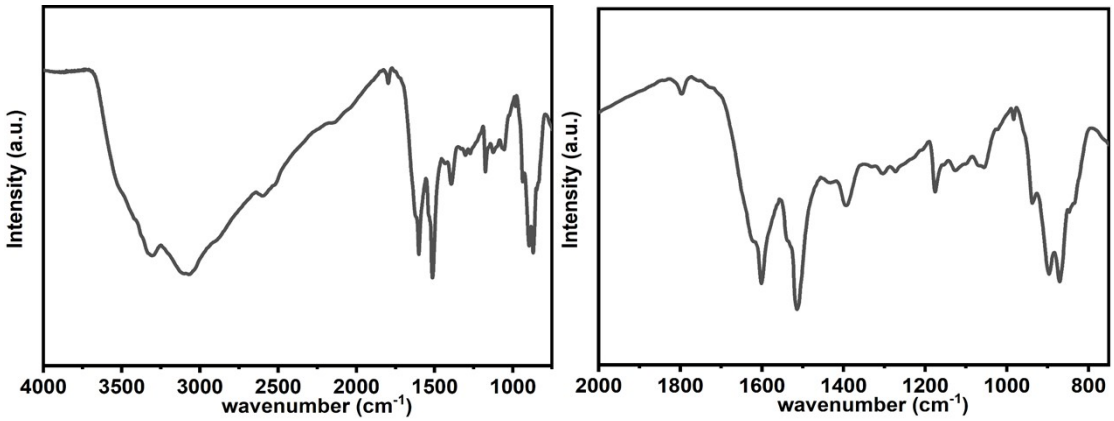

Figure S3 FTIR spectrum of DMoGC-0.

FTIR spectrum of DMoGC-0 was tested and compared with that of DMoGC-SDS and DMoGC-CTAB, which showed very similar patterns.

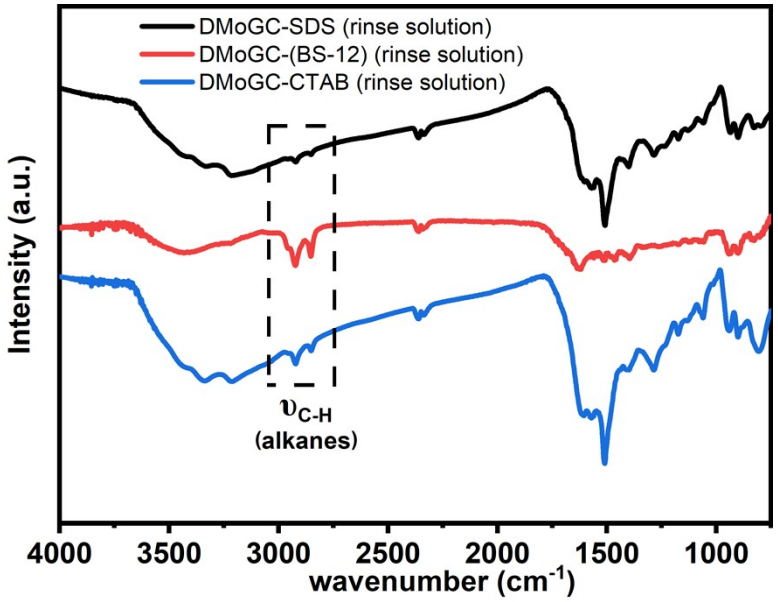

Fig. S4 FTIR spectrum of the rinse solution of DMoGC-SDS, DMoGC-(BS-12) and DMoGC-CTAB.

The obtained FTIR spectrum clearly present characteristic absorption peaks of aliphatic $–CH_2$, indicating the presence of surfactants in the rinse solution of the DMoGC samples.

Table S1. FTIR data analysis of different DMoGC samples.

Characteristic vibration	Wavenumber (cm^{-1})	Samples
υ_{N-H}	3380	DMoGC-(BS-12)
$\upsilon_{C-H(alkanes)}$	2921, 2852	DMoGC-(BS-12)
$\upsilon_{C=O}$	1624	DMoGC-SDS, DMoGC-(BS-12), DMoGC-CTAB
$\upsilon_{C=C(aromatic)}$	1600, 1510	DMoGC-SDS, DMoGC-CTAB, DMoGC-(BS-12)
$\delta_{C-H(alkanes)}$	1465	DMoGC-(BS-12)
$\upsilon_{C-N(amide)}$	1391	DMoGC-SDS, DMoGC-CTAB, DMoGC-(BS-12)
$\upsilon_{C-N(primary\ amine)}$	1326	DMoGC-(BS-12)
υ_{C-O}	1232	DMoGC-SDS, DMoGC-CTAB
$\upsilon_{C-N(N+)}$	1176	DMoGC-SDS, DMoGC-CTAB
$\upsilon_{O=P-O-}$	1074	DMoGC-(BS-12)
$\upsilon_{O=P-O-}$	1052	DMoGC-SDS, DMoGC-CTAB
$\upsilon_{Mo=O}$	938	DMoGC-SDS, DMoGC-CTAB
$\upsilon_{Mo-O-Mo}$	895, 869	DMoGC-SDS, DMoGC-CTAB
$\upsilon_{Mo-O-Mo}$	891	DMoGC-(BS-12)

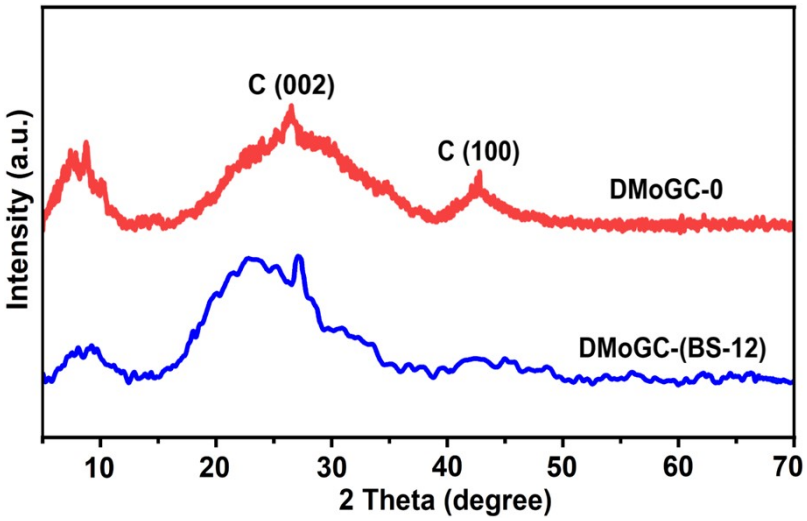

Figure S5. XRD patterns of DMoGC-0 and DMoGC-(BS-12).

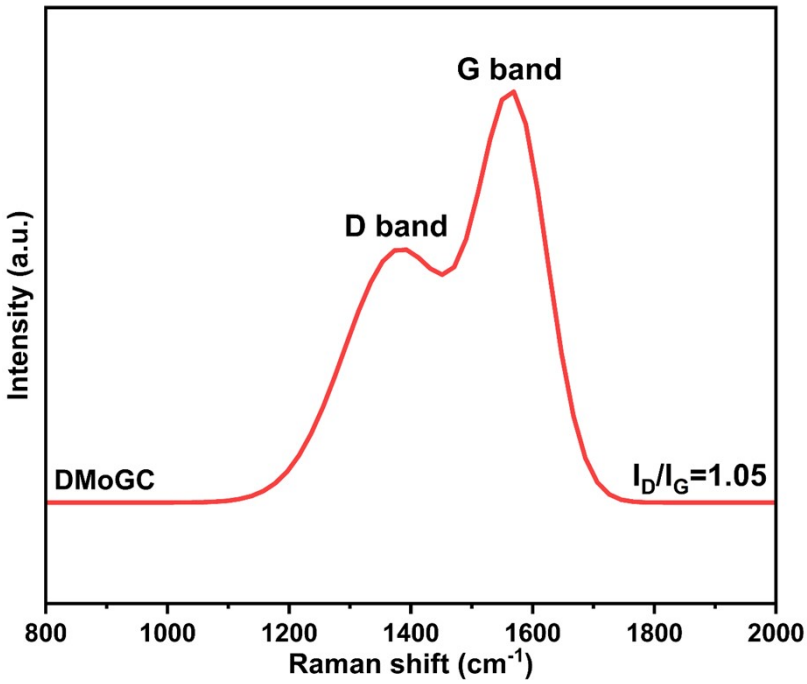

Figure S6. Raman spectrum of DMoGC-0.

Table S2. Textural parameters of different samples

Samples	S_{BET} [a] /$m^2 \cdot g^{-1}$	V_T [b] /$cm^3 \cdot g^{-1}$	S_{micro} [c] /$m^2 \cdot g^{-1}$	V_{micro} [d] /$cm^3 \cdot g^{-1}$	S_E [e] /$m^2 \cdot g^{-1}$	D [f] /nm
DMoGC-SDS	131.4	0.25	3.4	0.006	128.0	8.6
DMoGC-(BS-12)	74.6	0.14	0.5	0.001	73.1	15.5
DMoGC-CTAB	152.3	0.29	7.4	0.014	144.9	7.0

[a] BET surface area; [b] Total pore volume at (P/P_0) = 0.992; [c] t-Plot micropore area; [d] t-Plot micropore volume; [e] t-Plot external surface area; [f] average pore width.

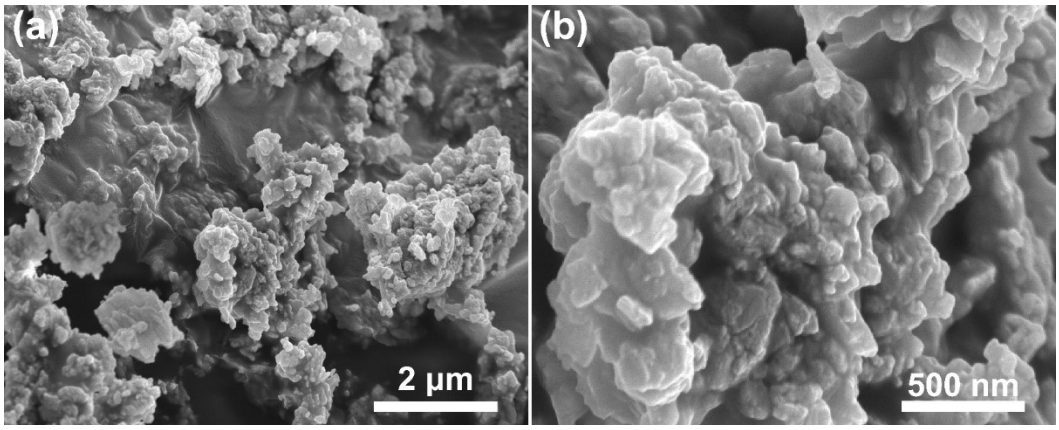

Figure S7. SEM images of PPD-PMo_{12}.

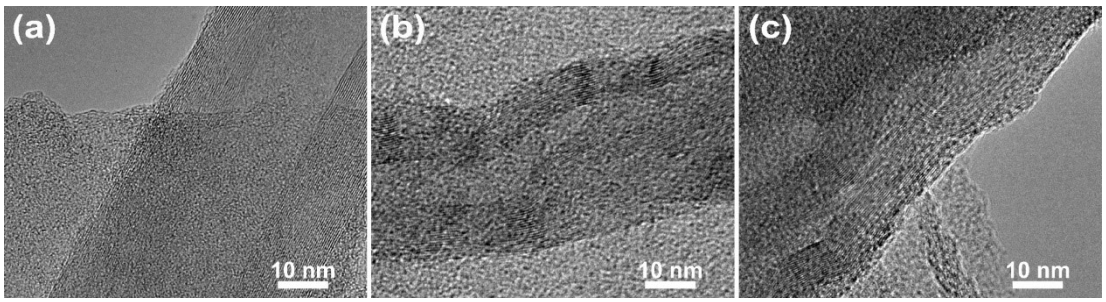

Figure S8. TEM images of (a) DMoGC-SDS, (b) and DMoGC-(BS-12) and DMoGC-CTAB.

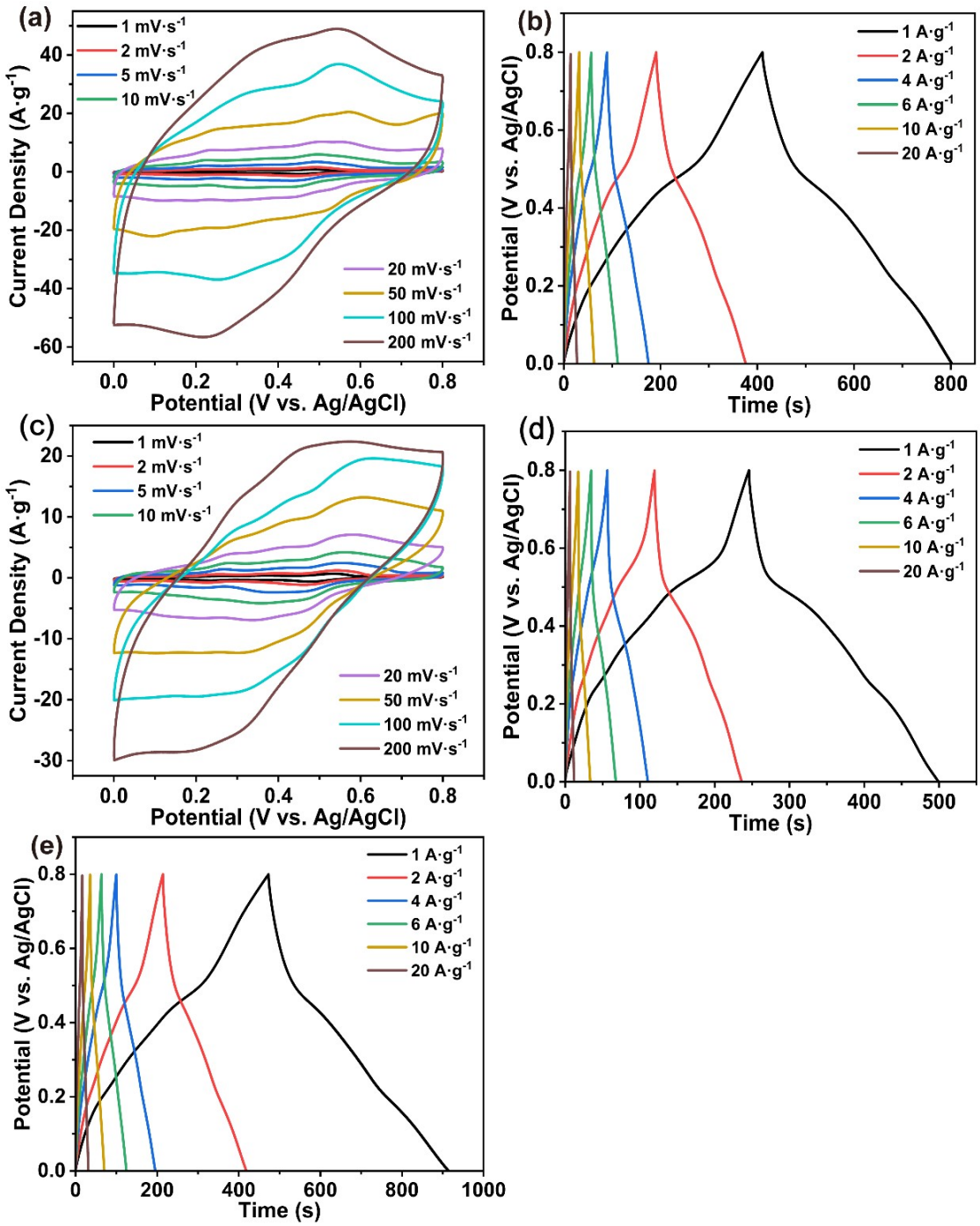

Figure S9. CV curves at scan rates from 1 to 200 $mV \cdot s^{-1}$ of (a) DMoGC-SDS electrode and (c) DMoGC-(BS-12) electrode; GCD curves at current densities from 1 to 20 $A \cdot g^{-1}$ of (b) DMoGC-SDS electrode, (d) DMoGC-(BS-12) electrode and (e) DMoGC-CTAB electrode.

Table S3. Capacitive performance of different DMoGC samples at different scan rates

Samples	Specific capacitance ($F \cdot g^{-1}$) at 1 $mV \cdot s^{-1}$	Specific capacitance ($F \cdot g^{-1}$) at 100 $mV \cdot s^{-1}$	Rate capability (%)
DMoGC-SDS	387	236	60.98
DMoGC-(BS-12)	275	124	45.09
DMoGC-CTAB	422	262	62.09

Capacitance contribution of surface-control and diffusion-control

The current response (i) at a fixed potential (V) can be described as the combination of two separate mechanisms, namely capacitive effects ($k_1 v$) and diffusion-controlled insertion ($k_2 v^{0.5}$). Therefore, the electrical double layer capacitance (C_{DL}) and the diffusion-controlled capacitance (C_D) for the aerogel electrode according to equation:

$$i(V) = k_1 v + k_2 v^{0.5} \quad (1)$$

where v is the scan rate, k_1 and k_2 are proportionality constants related to the capacitive and diffusion-limited processes, respectively. By determining both k_1 and k_2, it could distinguish the capacitive and diffusion capacitance, respectively. The calculated results are presented in **Table S4**.

Table S4. Calculated C_{EDL} and C_D of different DMoGC samples at different scan rates

Scan rates ($mV \cdot s^{-1}$)	DMoGC-SDS		DMoGC-(BS-12)		DMoGC-CTAB	
	C_{EDL} ($F\ g^{-1}$)	C_D ($F\ g^{-1}$)	C_{EDL} ($F\ g^{-1}$)	C_D ($F\ g^{-1}$)	C_{EDL} ($F\ g^{-1}$)	C_D ($F\ g^{-1}$)
1	174	213	66	209	211	211
2	174	207	65	195	211	204
5	174	195	65	180	211	190
10	174	189	66	172	211	183
20	174	180	70	148	211	174
50	174	114	77	86	211	101
100	174	62	81	43	212	51

Calculation of b value

According to equation (2) and (3):

$$i(v) = av^b \quad (2)$$

$$\log(i) = b\log(v) + \log a \quad (3)$$

where i is the current density, v is the scan rate, a and b are variables. The b value can be determined from the slope of $\log(i)$ versus $\log(v)$ plot.

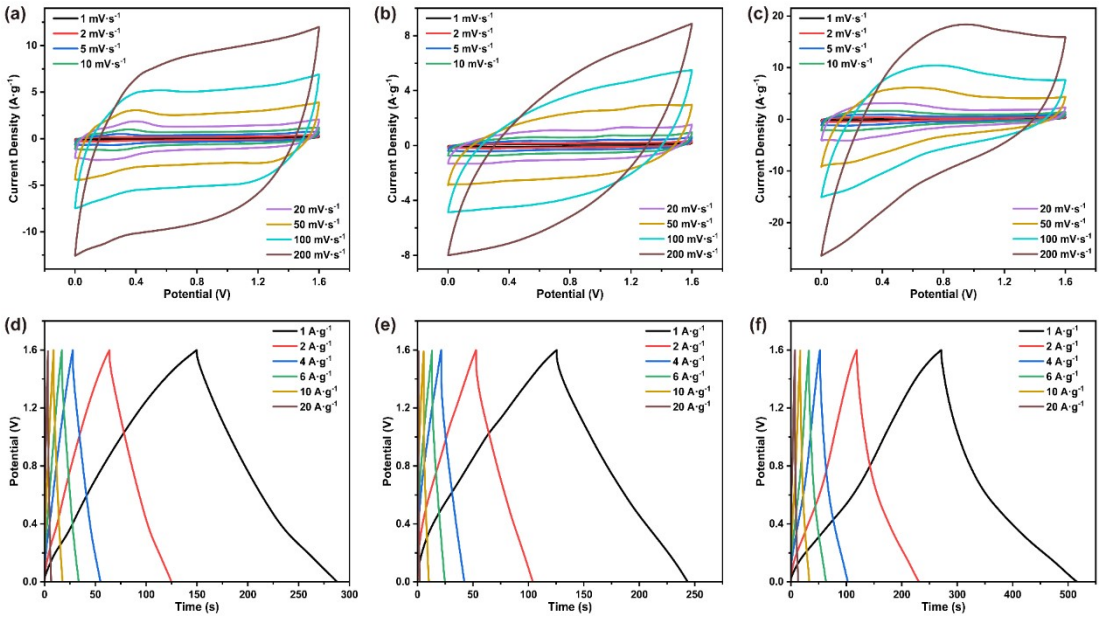

Figure S10. CV curves at scan rates from 1 to 200 $mV \cdot s^{-1}$ of (a) DMoGC-SDS SSC, (b) DMoGC-(BS-12) SSC and (c) DMoGC-CTAB SSC. GCD curves at current densities from 1 to 20 $A \cdot g^{-1}$ of (d) DMoGC-SDS SSC, (e) DMoGC-(BS-12) SSC and (f) DMoGC-CTAB SSC.

Table S5. Capacitive performances of SSC based on different DMoGC composites at different scan rates

Samples	Specific capacitance ($F \cdot g^{-1}$) at 1 $mV \cdot s^{-1}$	Specific capacitance ($F \cdot g^{-1}$) at 200 $mV \cdot s^{-1}$	Rate capability (%)
DMoGC-SDS	100	41	41.03
DMoGC-(BS-12)	89	25	28.09
DMoGC-CTAB	153	65	42.61